Chemical Geology 610 (2022) 121103

Contents lists available at ScienceDirect

Chemical Geology

journal homepage: www.elsevier.com/locate/chemgeo

Cold-seep carbonates of the Laptev Sea continental slope: Constraints from fluid sources and environment of formation

Alexey Ruban [a,*], Maxim Rudmin [a], Alexey Mazurov [a], Denis Chernykh [b], Oleg Dudarev [b], Igor Semiletov [b,c]

[a] Division for Geology, School of Earth Sciences & Engineering, Tomsk Polytechnic University, 634050 Tomsk, Russia
[b] V.I. Il'ichev Pacific Oceanological Institute, Far Eastern Branch of the Russian Academy of Sciences, 690041 Vladivostok, Russia
[c] Tomsk State University, 634050 Tomsk, Russia

ARTICLE INFO

Keywords:
Authigenic carbonates
Cold seep
Stable oxygen and carbon isotopes
Trace element enrichments
Redox conditions
Laptev Sea

ABSTRACT

This study presents results of the petrographic, mineralogical, stable isotopes of oxygen and carbon, and trace element investigation of authigenic carbonates collected at newly discovered active cold seeps on the Laptev Sea continental slope at ~300 m water depth. These carbonates are mainly represented by Mg-calcite with $MgCO_3$ content from 9.1 mol% to 14.0 mol%. The low $\delta^{13}C$ values of carbonates ranging from −50.6 ‰ to −32.4 ‰ (V-PDB) indicate that they were formed from anaerobic oxidation of biogenic methane and minor participation of other carbon sources. The difference between measured (from 4.7 ‰ to 5.5 ‰) and calculated (4.0 ‰) $\delta^{18}O_{carb}$ values might be inherited from fluids enriched in ^{18}O due to dissociation of gas hydrates, which could be the source of methane. The carbonates exhibit weak enrichment in Co, moderate and strong enrichments in As, Mo, and Sb, and strong enrichment in U. Interestingly, As, Sb, and Co correlate with the pyrite content. This indicates that authigenic iron sulfides promote the immobilization of these redox-sensitive elements in seep sediments. The $(Mo/U)_{EF}$ values and anomalies of concentration of Mo and U probably indicate variations in the redox conditions during carbonate formation due to episodically seepage activity changes. Ascending methane-bearing fluids were the main contributor to the enrichment of cold-seep carbonates in As, Mo, Sb, and U at the Laptev Sea continental slope. However additional input from the particulate shuttle process can not be ruled out.

1. Introduction

Authigenic carbonates occur in the seas of the Arctic Ocean much less frequently than in the seas of humid and arid zones, which is explained by the increased solubility of carbon dioxide due to low water column temperatures (Bates et al., 2009; Guinotte and Fabry, 2008). However, authigenic carbonates found in various parts of the Arctic seas (inner shelf, outer shelf, continental slope) have been documented by many authors (Himmler et al., 2019; Kravchishina et al., 2017; Mazzini et al., 2016; Schier et al., 2021; Schubert et al., 1997; Thiagarajan et al., 2020).

Microbial carbonates are a unique geological archive of biogeochemical processes and environmental conditions since, during their formation, the isotopic composition of the "parent" carbon is inherited to varying degrees, and various redox-sensitive trace elements are also captured (Hood and Wallace, 2018; Smrzka et al., 2021; Zhou et al., 2016). Depending on the carbon source, different types of carbonates are distinguished, for example, (i) diagenetic carbonates formed during the microbial decomposition of sedimentary organic matter (Allouc, 1990; Kelts and McKenzie, 1982; Lein, 2004); (ii) carbonates formed during the anaerobic oxidation of methane of various type: abiogenic, biogenic (including methane from gas hydrates), thermogenic, and their mixing (Botz et al., 2002; Peckmann et al., 2001; Ruban et al., 2020); (iii) carbonates formed due to oil biodegradation (Feng et al., 2009; Mansour and Sassen, 2011; Naehr et al., 2009; Roberts et al., 2010). Cold-seep carbonates are formed under sulfate-driven anaerobic oxidation of methane (SD-AOM), controlled by a consortium of sulfate-reducing bacteria and methane-oxidizing archaea. Such conditions are typical for cold seep sites, where methane-rich (or other hydrocarbons) fluids in chemical non-equilibrium with seawater are transported through the sub-seafloor environment either along faults and fractures or through the porosity of sediments and are released at the sediment–seawater interface (Naehr et al., 2007). The sulfate-methane transition zone (SMTZ) can be situated close to the sediment-water interface when there

* Corresponding author.
E-mail addresses: ruban@tpu.ru (A. Ruban), rudminma@tpu.ru (M. Rudmin), akm@tpu.ru (A. Mazurov), dudarev@poi.dvo.ru (O. Dudarev).

https://doi.org/10.1016/j.chemgeo.2022.121103
Received 30 May 2022; Received in revised form 7 September 2022; Accepted 7 September 2022
Available online 12 September 2022

is a high flow of upward migrating methane-bearing fluid (Regnier et al., 2011; Teichert et al., 2005). The Arctic is characterized by elevated concentrations of methane in the atmosphere (approximately 1.85 ppm; Shakhova et al., 2010). Methane is a strong greenhouse gas, therefore its emission to the atmosphere can lead to positive feedback on climate warming. SD-AOM, which contributes to the precipitation of carbonates, is the main mode of oxidation of methane in the marine sedimentary environment which limits methane release into the atmosphere (Boetius et al., 2000).

Due to the anaerobic oxidation of hydrocarbon gases (including methane), the produced dissolved inorganic carbon leads to the increase of the alkalinity of pore water (Baker and Burns, 1985; Kulm et al., 1986). In the presence of calcium and magnesium cations from seawater, elevated carbonate alkalinity promotes the precipitation of carbonates, which are characterized by the low isotopic composition of carbon because they are issued from methane and other hydrocarbons (Berner, 1980; Luff et al., 2004; Peckmann et al., 2001). Cold-seep carbonates show a wide range of mineralogical compositions that include high-Mg calcite (HMC) and low-Mg calcite (LMC), dolomite, aragonite, siderite (Matsumoto, 1990; Aloisi et al., 2000; Feng et al., 2009; Tong et al., 2013; Guan et al., 2019; Naehr et al., 2000; Lu et al., 2018). The mineralogy of carbonates indicates whether they were formed close to the seafloor (aragonite) or rather in deeper sediments (calcite, Mg-calcite, dolomite; Aloisi et al., 2000; Bohrmann et al., 1998; Haas et al., 2010; Yao et al., 2021). In addition, HMC and dolomite can point at high contents of dissolved sulfide in pore water during carbonate formation (Lu et al., 2018, 2021). Authigenic carbonates can have various shapes, for example, crusts, slabs, nodules, chimneys, and sometimes massive pavements (e.g., Aloisi et al., 2000; Bayon et al., 2009; Feng and Chen, 2015; Mansour and Sassen, 2011; Sun et al., 2020). Previous studies of the Laptev Sea authigenic carbonates have shown that carbon from various sources participates to their formation: biogenic methane, thermogenic methane, and organic matter of bottom sediments (Kravchishina et al., 2017; Krylov et al., 2015; Logvina et al., 2018; Ruban et al., 2020).

Carbonate minerals, including calcite, aragonite, and dolomite, are highly prone to incorporate significant amounts of trace elements (Veizer, 1983). Systematic analysis of trace element contents and ratios can provide a reliable reconstruction of the environment shaped by biogeochemical processes, temporal changes in fluid composition, fluid flow, and redox conditions (Smrzka et al., 2020). Early studies focused mainly on the content of magnesium, strontium, iron, and manganese, however more unconventional trace elements such as molybdenum, uranium, arsenic, and antimony can yield more valuable information on the carbonate formation at seeps. Additionally, SD-AOM also causes an increase in the concentration of hydrogen sulfide in pore waters (e.g., Li et al., 2019). It commonly results in the precipitation of iron monosulfide or polysulfide minerals (e.g., mackinawite and greigite respectively), which eventually convert into pyrite (e.g., Wilkin and Barnes, 1996).

This paper presents the results of petrographic, mineralogical, and geochemical studies of authigenic carbonates sampled from a little-known cold seep site on the continental slope of the Laptev Sea. We analyzed the oxygen and carbon isotopic compositions and the trace elements content to assess the formation conditions of these cold-seep carbonates.

2. Site location and geological setting

The Laptev Sea is an epicontinental sea bounded by the Taimyr Peninsula from the west and the New Siberian Islands from the east. The sea area is estimated at 673000 km^2, and the maximum depth reaches 3385 m in the Nansen Basin. 70% of the sea area is represented by a shelf with a depth of fewer than 100 m (Bogoyavlensky et al., 2018a). The shelf break runs along the 100 m isobath, below which is the continental slope.

The Laptev Sea basin is located at the junction of three large tectonic structures of different ages: the ancient Siberian platform, the Mesozoic Verkhoyansk–Kolyma fold system, and the young Eurasian oceanic basin with the Gakkel Ridge (Daragan-Sushchova et al., 2021). According to some estimates (Bogoyavlensky et al., 2022; Daragan-Sushchova et al., 2021), the thickness of the Upper Cretaceous-Cenozoic sedimentary cover reaches 13–16 km, which has the potential to generate hydrocarbons (Polyakova and Borukaev, 2017). The sedimentary cover is disrupted by numerous faults with a displacement amplitude of up to 2 km that form the Laptev Sea Rift System (LSRS; Drachev, 2002; Sekretov, 2002). On the shelf break, LSRS intersects with the Khatanga-Lomonosov Fracture Zone (KLFZ) extending in the SW–NE direction. KLFZ was considered by new multichannel seismic data as a transform fault formed during the Paleocene (Shipilov et al., 2019). The LSRZ and KLFZ faults can play a major role in methane migration at previously discovered seeps (Sergienko et al., 2012; Shakhova et al., 2019; Shakhova et al., 2015) on the outer shelf of the Laptev Sea (Bogoyavlensky et al., 2022).

The study area, where the carbonate crusts were obtained, is located within the upper continental slope of the western Laptev Sea. Four seismic sections (LS0914, LS0923, LS0924, LS0927) were acquired in this part of the continental slope by CJSC MAGE from the R/V “Geolog Dmitry Nalivkin” in 2009 (Bogoyavlensky et al., 2018a). Results of seismic section analysis demonstrate the presence of numerous acoustic anomalies with gas saturation signs in Middle Miocene–Quaternary sediments of the sedimentary cover. Tops of these anomalous objects lie at a depth of about 100–200 m below the seabed. Besides, a few bottom simulating reflectors (BSR) serve as indirect evidence of gas hydrate are recognized in the Laptev Sea section. It probably corresponds to the bottom of the gas hydrate stability zone overlying free gas deposits (Bogoyavlensky et al., 2018a, 2018b). Widespread faults can serve as pathways for gas migration from the lower gas-saturated sediment strata to the upper sediment strata, as was stated for the Laptev Sea outer shelf.

3. Sampling and methods

3.1. Study area and sampling

Authigenic carbonates from seep sites in the western part of the Laptev Sea continental slope were obtained during the 82nd research cruise of the RV «Akademik Mstislav Keldysh» in 2020. Sediment samples containing authigenic carbonate were collected at station AMK-6939 (station coordinates are 77°17′4“N and 122°5’45” E, water depth is 294 m; Fig. 1A) using a grab sampler. The sampling depth of the grab used is approximately 40 cm below the seabed, and it indicates the presence of carbonates in the upper near-surface horizon of sediment. A lot of carbonate nodules with sizes up to ~7–9 cm were found during the washing of the grab corer sample. Carbonates were washed to remove attached uncemented sediments and dried at 60 °C before analysis. Carbonate samples for stable carbon and oxygen isotope measurements, inductively coupled plasma mass spectrometry (ICP-MS), X-ray fluorescence (XRF), and X-ray diffraction (XRD) were carefully ground to a fine powder using an agate mortar.

Hydroacoustic investigations were performed using a Kongsberg EA600 ship-mounted single-beam echosounder operating at a frequency of 12 kHz and emitting an acoustic signal with a period of 0.5 Hz, and a pulse width of 0.512 ms. The speed of the research vessel at the time of registration of the gas flare was 9.2 knots, the heading was 272°. The gas flares were recorded <1 km from the sampling station (Fig. 1B).

3.2. Petrography and mineralogy of carbonates

Polished thin sections from studied carbonate samples were prepared to identify the main carbonate phases. Thin section petrography was conducted on a CARL ZEISS Axio Imager 2 polarization microscope coupled to AxioCam MRc5 camera, using the Axio Vision 4.8 for image

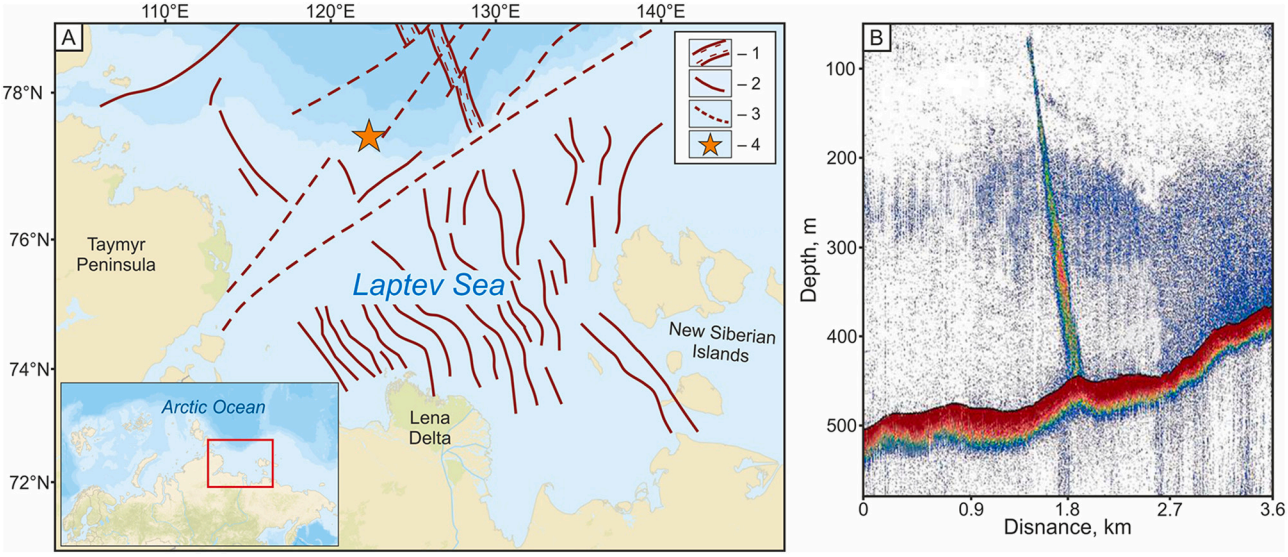

Fig. 1. (A) Location of sampling site and main faults in the basement and sediment cover according to Baranov et al., 2020; Drachev, 2000; Sekretov, 2002: 1 – the Gakkel Ridge valley; 2 – normal faults; 3 – transform and strike slip faults; 4 – seep site where authigenic carbonates were obtained. (B) Hydro-acoustical images of a detected gas flare.

analysis and camera control. Some polished thin sections and carbonate fragments were examined with TESCAN VEGA 3 SBU (TESCAN, Brno, Czech Republic) scanning electron microscope (SEM) with an OXFORD X-Max 50 (OXFORD Instruments, High Wycombe, UK) energy-dispersive adapter (EDS) under following parameters: a 20 kV accelerating voltage, specimen current of 4–12 nA and a spot diameter of approximately 0.1–2 μm. Thin sections and carbonate fragments were fixed to a double-sided carbon conductive tape placed on an aluminum stub before analysis.

The bulk mineralogical composition of authigenic carbonates was determined using a Bruker D2 Phase X-ray diffractometer (Billerica, MA, USA) equipped with a Cu-Kα radiation source and operated at a current of 10 mA and a voltage of 30 kV. The finely powdered samples were scanned from 5° to 70° 2θ using a step of 0.02° at a scanning rate of 2 s per step. The diverging, scattering, and receiving slits were 1 mm, 3 mm, and 0.3 mm, respectively. BRUKER Diffrac EVA, PDF4 Mineral database of ICDD, and the Crystallographic Open Database (COD) were used for mineral identification by automatic and manual peak search. Mineral quantification was performed by Rietveld refinement using the TOPAS 5 software.

From the d104 values of Mg-calcite, content in mol % $MgCO_3$ was calculated using a linear interpolation between interplanar spacings of stoichiometric dolomite (d_{104} = 2.886 Å) and stoichiometric calcite (d_{104} = 3.035 Å; Goldsmith et al., 1961; Pierre et al., 2012). $MgCO_3$ contents were calculated by a linear empirical equation (Zhang et al., 2010), which yields $d_{104} = -0.003 * MgCO_3$ mol% + 3.035 (Goldsmith et al., 1961; Markgraf and Mineralogist, 1985; Smrzka et al., 2021).

3.3. Stable carbon and oxygen isotopic analyses

The stable carbon and oxygen isotope ratios of the bulk nine carbonate samples were performed at the Laboratory of isotope and elemental analysis in Kazan (Volga region) Federal University (Russia). For analysis, powdered carbonate samples (approximately 200 μg) were treated with 100% phosphoric acid at 70 °C to release CO_2 for measurements using a Delta V Plus mass spectrometer (Thermo Fisher Scientific, Bremen, Germany). The $\delta^{13}C$ and $\delta^{18}O$ values obtained are reported in standard δ notation relative to the Vienna Peedee belemnite (V-PDB) standard. Reproducibility was checked by replicate analysis of laboratory standards and was ±0.07‰ for both carbon and oxygen isotope analyses. The equilibrium $\delta^{18}O$ values of calcite precipitated under present-day seafloor conditions were calculated with the equation of Kim and O'Neil (1997):

$$1000ln\alpha_{(calcite-water)} = 18.03^{*}(10^{3}\ T^{-1}) - 32.42,$$

where T is bottom water temperature in Kelvins. Calcite/water fractionation factor α was calculated using the formula (Deininger et al., 2021):

$$\alpha_{calcite/water} = \left(1000 + \delta^{18}O_{calciteV-SMOW}\right)/\left(1000 + \delta^{18}O_{waterV-SMOW}\right).$$

The conversion of $\delta^{18}O$ values from V-PDB to V-SMOW scales was calculated according to the equation (Coplen et al., 1983):

$$\delta^{18}O_{V-PDB} = 0.97002\delta^{18}O_{V-SMOW} - 29.98.$$

3.4. Major and trace elements

The major element concentrations of the nine carbonate samples were estimated using a HORIBA XGT 7200 X-ray fluorescence (XRF) microscope (Horiba, Kyoto, Japan) operated at a tube current of 1 mA, with a 1.2 mm X-ray beam diameter for 100 s and a voltage of 50 kV. For XRF analysis, bulk powdered carbonates were pressed in pellets at a pressure of 25 MPa and fused at a temperature of 900 °C. The average value was calculated from three measurement points evenly distributed on each pellet surface. The detection limit for major elements was better than 0.01 wt%. For XRF data, detrital contents in the carbonate crusts were estimated simply by summing the contents of Al_2O_3, SiO_2, K_2O, TiO_2, and Fe_2O_3 (Bayon et al., 2009). The trace element concentrations were measured on nine carbonate samples using inductively coupled plasma-mass spectroscopy (ICP-MS), conducted on ELAN DRC-e (PerkinElmer Inc., Waltham, MA, United States) instrument. About 0.5 g of the bulk powdered carbonate was dissolved by a mixture of HNO_3 and HF. Precision and accuracy were better than 5% for major elements and 10% for trace elements.

The enrichment factor (EF) was used to assess the authigenic enrichment in trace elements during carbonate formation. EF was calculated using the standard formula (Tribovillard et al., 2006): $EF_{elementX} = [(X/\ Al)_{sample}/(X/Al)_{upper\ crust}]$, where X and Al represent the weight concentrations of the considered element (X) and aluminum (Al) normalized using the Earth's upper crust compositions (McLennan, 2001). $EF_X > 1$ indicates enrichment in element X relative to its average crustal abundance. In practical terms, EFs > 3 represents a detectable

enrichment in an element over average crustal concentrations, and EFs > 10 represent a moderate to a strong degree of enrichment (Algeo and Tribovillard, 2009).

4. Results

4.1. Mineralogy and thin section petrography

Typical macroscopic features of authigenic carbonate samples are shown in Fig. 2. Studied carbonates are mainly represented by three following varieties: tubular concretions (Fig. 2A), isometric crusts (Fig. 2B), and spherical or elliptical nodules (Fig. 2C) with sizes up to 10 cm. They have gray colour, dense and strongly cemented texture, and a low degree of porosity. The size of hollow channels and cavities does not exceed 0.5 mm in width. Carbonate crusts consist of the microcrystalline carbonate matrix that lithifies detrital minerals of host sediments and singular bivalve shell fragments. Dark bands reflect the uneven distribution of clay minerals in the gray groundmass of carbonates (Fig. 2D; Fig. 3A and B). According to the XRD data (Table 1), carbonate minerals are represented by Mg-calcite, dolomite, and kutnohorite (CaMn $(CO_3)_2$). Total carbonate content varies from 32.8% to 52.1%. The detrital fraction consists of quartz (22.1–27.9%), feldspar (11.7–24.8%), and clay minerals (11.2–20.3%). Quartz and feldspars are represented by rounded silt-sized grains randomly scattered within the carbonate matrix (Fig. 3C and D). The microcrystalline carbonate matrix is mainly composed of an aggregate of Mg-calcite and clay minerals. The EDS analysis results show that the Mg content in Mg-calcite ranged mainly from 2 to 7 wt%. However, small areas (about ~15 × 15 μm) with Mg content up to 18% were found (Fig. 5C and D). d_{104} values of bulk carbonate sample are between 2.993 Å and 3.008 Å and calculated values of $MgCO_3$ content ranged from 9.1 mol% to 14.0 mol%.

Various authigenic pyrite aggregates are associated with Mg-calcite such as isolated framboids, framboids with radial overgrowths like sunflowers in shape (up to 70 μm in diameter; Fig. 4C), and euhedral pentagonal dodecahedron crystals (approximately 15 μm in width; Fig. 4D), which infill cavities or organisms (Fig. 4E). These aggregates are composed of numerous smaller particles approximately from 0.5 μm to 1 μm in diameter, and form bands have a length of up to 500 μm.

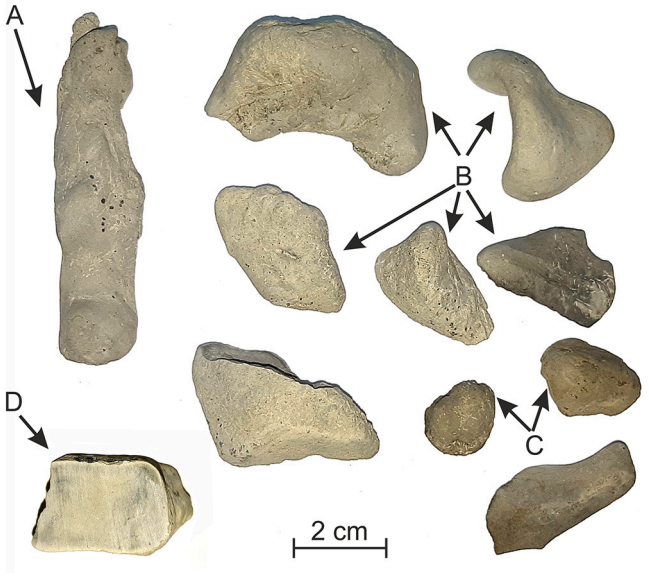

Fig. 2. Typical morphologies of authigenic carbonates from the Laptev Sea continental slope: tubular concretions (A), isometric crusts (B), spherical and elliptical nodules (C), cross-sections through carbonate crust (D).

4.2. Isotope geochemistry, major and trace elements

Stable carbon and oxygen isotopic compositions of authigenic carbonates are listed in Table 1 and reported in Fig. 6. All carbonate samples studied have negative $\delta^{13}C$ values and positive $\delta^{18}O$ values. The $\delta^{13}C$ values range from −50.6 ‰ to −32.4 ‰ V-PDB, whereas the $\delta^{18}O$ values vary from 4.7 ‰ to 5.5 ‰.

Contents of major and selected trace elements in studied bulk carbonate samples are listed in Table 2 and reported in Figs. 7, 8, 9, 10. Al_2O_3 contents range from 7.43% wt% to 9.75 wt% with an average of 8.48 wt%. The predominance of SiO_2 in samples is apparent with contents from 23.6 wt% to 35.0 wt%. Contents of MgO, CaO and MnO range from 3.51 wt% to 4.34 wt% for MgO, 22.0 wt% to 30.6 wt% for CaO and 0.06 wt% to 0.17 wt% for MnO. For both EDS and XRF data, Mg/Ca (MgO/CaO) ratio ranges from 0.06 to 0.80 and from 0.13 to 0.17, respectively. According to XRF data (Table 2), detrital contents in carbonate crusts vary from 34.8 to 50.1 wt%, indicating that terrigenous clay-rich material is incorporated within the carbonate matrix during the carbonate precipitation.

The contents of Cr, Co, Cu, Ni, Zn, Ba, and Th range from 22.3 ppm to 54.7 ppm for Cr, 21.0 ppm to 55.8 ppm for Ni, 180 ppm to 290 ppm for Ba, 3.45 ppm to 6.32 ppm for Th. Co, Cu, and Zn contents display narrow ranges from 21.1 ppm to 28.8 ppm, 13.7 ppm to 21.2 ppm, and 44.4 ppm to 59.1 ppm, respectively. The maximum Ni, Sr, and Mo contents are associated with sample 6939/2, which is characterized by the highest $\delta^{13}C$ value (−32.4 ‰). Moderate to strong enrichments in As (As_{EF} from 2.2 to 42.3), Sb (Sb_{EF} from 2.8 to 15.3), Sr (Sr_{EF} from 3.21 to 5.62), and Mo (Mo_{EF} from 9.0 to 25.0) are observed in studied carbonates, and only U (U_{EF} from 12.3 to 22.7) exhibit strong enrichments in all nine analyzed samples. Some others trace elements (Co, Cu, Zn) display enrichment factors between 1 and 3.

5. Discussion

5.1. Fluid source for carbonate precipitation

The compositions of stable isotopes of carbon and oxygen, as well as the structure and mineralogy of cold-seep carbonates, are indicators of the fluid sources (e.g., Feng and Chen, 2015; Peckmann et al., 2001; Roberts et al., 2010; Smrzka et al., 2019b). Carbonates formed during SD-AOM have extremely low $\delta^{13}C$ values because $\delta^{13}C$ values of biogenic and thermogenic methane range from −110 ‰ to−50 ‰ (Whiticar et al., 1986) and from −50 ‰ to −30 ‰ (Sackett, 1978), respectively. However, $\delta^{13}C$ values of carbonates cannot be simply equated with methane because there is a mixing of carbon from different sources include dissolved inorganic carbon from seawater, decomposed organic matter, and carbon deriving from the oxidation of hydrocarbons (Peckmann and Thiel, 2004), which hampers the identification of the parent carbon composition. Despite this, the carbon isotope composition of cold-seep carbonates is a reliable indicator for estimating the main source of methane (e.g., Himmler et al., 2015; Peckmann and Thiel, 2004; Roberts et al., 2010; Tong et al., 2013).

The very low $\delta^{13}C$ values of studied carbonates suggest that methane is the main source of carbon. The results (Table 1; Fig. 6) show a significant range of carbon isotopic values, that probably reveal a mixing of biogenic methane with carbon from other sources, which can hypothetically be decomposed organic matter, dissolved inorganic carbon from seawater, thermogenic methane and other heavier hydrocarbons. It is unlikely that the organic matter of sediments could significantly participate in the carbonate precipitation and influence its carbon isotope composition since the content of total organic carbon in sediments of this part of the Laptev Sea continental slope ($\delta^{13}C$ ~ −25 ‰ to −22 ‰ V-PDB) is <1% (Logvina et al., 2018; Martens et al., 2020). Fig. 6 demonstrates that authigenic carbonates from the continental slope of the Laptev Sea are characterized by lighter $\delta^{13}C$ than previously studied carbonates from the Laptev Sea shelf.

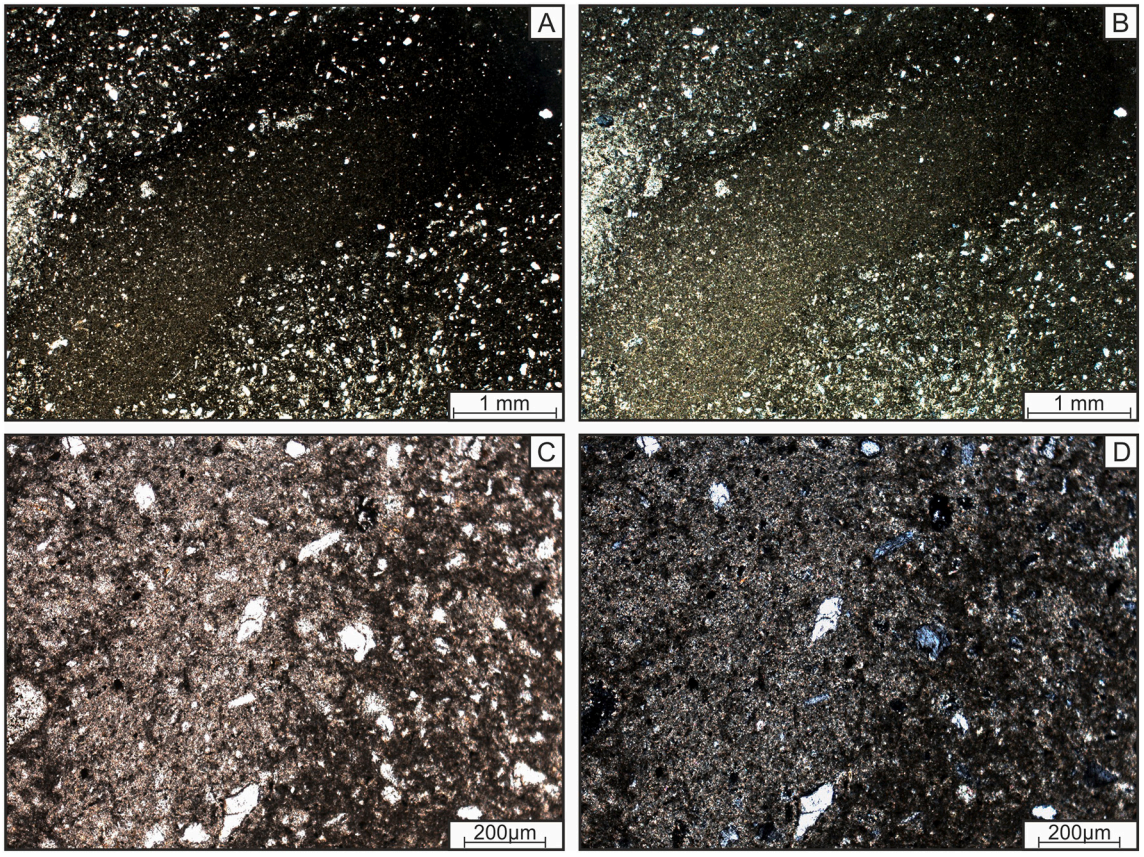

Fig. 3. Thin-section photomicrographs in plane- (left) and cross- (right) polarized light of authigenic carbonates from continental slope of Laptev Sea. (A and B) Banded structure of the microcrystalline carbonate cement reflecting the uneven distribution of clay minerals. (C and D) Detrital mineral fragments (mainly quartz and feldspar) in the microcrystalline carbonate cement.

Table 1
Mineralogical compositions and carbon and oxygen stable isotope compositions of the studied authigenic carbonates from the continental slope of Laptev Sea.

	Q	FSP	Clay	Pyr	Carbonates			$MgCO_3$	$\delta^{13}C$	$\delta^{18}O$
					MC	Dol	Kut			
	%							mol %	‰	
6939/1	23.9	24.8	16.6	1.8	31.6	1.3	–	14.0	−41.9	5.1
6939/2	25.2	13.4	17.7	1.9	32.6	1.9	7.3	8.5	−32.4	4.9
6939/3	22.7	11.7	11.9	1.5	51.2	1.0	–	9.1	−42.9	5.0
6939/4	23.8	12.1	12.3	1.5	49.4	0.9	–	10.1	−49.9	5.2
6939/5	22.8	11.9	20.3	1.2	40.1	1.0	2.7	10.9	−41.8	5.5
6939/6	27.9	14.1	16.2	2.5	34.1	1.8	3.4	9.6	−35.8	4.7
6939/7	23.7	12.8	14.5	1.1	44.8	1.2	1.9	10.3	−43.6	5.3
6939/8	25.6	13.9	11.2	1.3	45.5	0.8	1.7	9.9	−50.2	5.2
6939/9	22.1	11.9	12.9	1.0	49.7	0.9	1.5	9.9	−50.6	5.1

Q –quartz, FSP – feldspar, Clay – clay minerals, Pyr – pyrite, MC – Mg-calcite, Dol – dolomite, Kut – kutnohorite.

The oxygen isotope composition of the authigenic carbonates provides additional information about temperature during precipitation and the $\delta^{18}O$ values of the fluid source in which the carbonates precipitated (Greinert et al., 2001). The $\delta^{18}O$ values of the studied carbonates vary in a narrow range from 4.7‰ to 5.5‰ (Table 1), indicating the absence of significant fluctuations in the bottom water temperature and of the $\delta^{18}O$ value of the fluids during carbonate precipitation. The theoretical $\delta^{18}O$ values of Mg-calcite were calculated using the equilibrium equation of Kim and O'Neil (1997) and the following parameters: for bottom water $\delta^{18}O = 0.2$ ‰ (Bauch et al., 2016; Dubinina et al., 2019) and temperature is 0.1 °C (Chuvilin et al., 2022). The correction factor of +0.06 ‰ per mol % $MgCO_3$ was applied according to Tarutani et al. (1969). The calculated value of $\delta^{18}O$ for Mg-calcite with an average $MgCO_3$ content of 10.7 mol% in equilibrium with the bottom water is 4.0 ‰, thus lower by about 1% than those measured in the studied carbonates (Table 1, Fig. 6). Higher $\delta^{18}O$ values point to the participation of ^{18}O enriched fluid relative to pore water during carbonate precipitation. At cold seep sites, ^{18}O enrichment in the fluid can be caused by processes such as dehydration of clay minerals in deeper sediments (e.g., smectite-illite transformation; Hensen et al., 2004; Hesse, 2003), destabilization of gas hydrates (Davidson et al., 1983; Hesse and Harrison, 1981), deep-sourced fluids coming from oil and/or gas fields (Sofer and Gat, 1975). It is known that gas hydrate water is enriched by ^{18}O about 3‰ relative to pore water non-affected dissociation of gas hydrate (Crémière et al., 2012; Hesse and Harrison, 1981; Ussler and Paull, 1995). Seismic data demonstrate the presence of numerous acoustic anomalies with gas saturation signs and BSR horizon in sediments of the Laptev Sea continental slope (Bogoyavlensky et al., 2022;

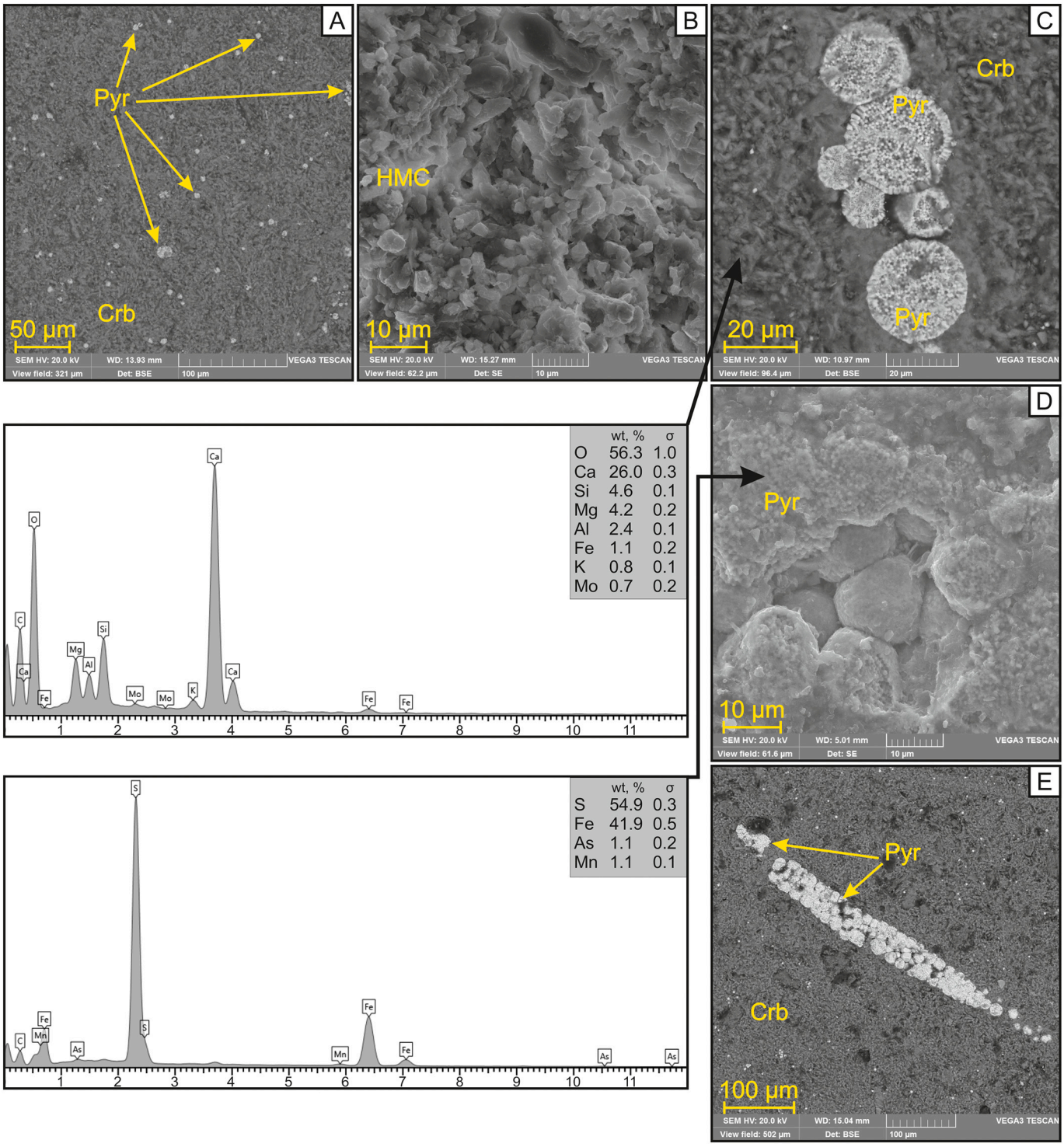

Fig. 4. Scanning electron microscope (SEM) images illustrating the internal structure of authigenic carbonates (A) Distribution of pyrite framboids in the microcrystalline carbonate cement: Pyr – pyrite, Crb – carbonate cement. (B) Finely crystalline high magnesian calcite: HMC – high magnesian calcite. (C) Concentration "sunflowers" aggregates of authigenic pyrite in carbonate cement: Pyr – pyrite, Crb – carbonate cement. (D) Euhedral pentagonal dodecahedron crystals of authigenic pyrite: Pyr – pyrite. (E) Massive pyrite framboids forming band aggregates Pyr – pyrite, Crb – carbonate cement. "ds".

Bogoyavlensky et al., 2018a, 2018b), which may indicate the presence of gas hydrate. Unfortunately, it is impossible to reliably estimate the individual contribution of these sources from the $\delta^{18}O$ values of carbonates. However, their combination can affect the enrichment of the carbonate-precipitating pore fluid by the $\delta^{18}O$.

5.2. Environmens of methane derived carbonate precipitation

The mineralogical composition of precipitating carbonates is controlled by thermodynamic and kinetic factors, including the Ca^{2+}/Mg^{2+} ratios, temperature, alkalinity, sulfate concentration, carbonate saturation state, and the degree of microbial activity (Burton, 1993; Luff et al., 2004; Naehr et al., 2000). The mineralogy of cold-seep carbonates

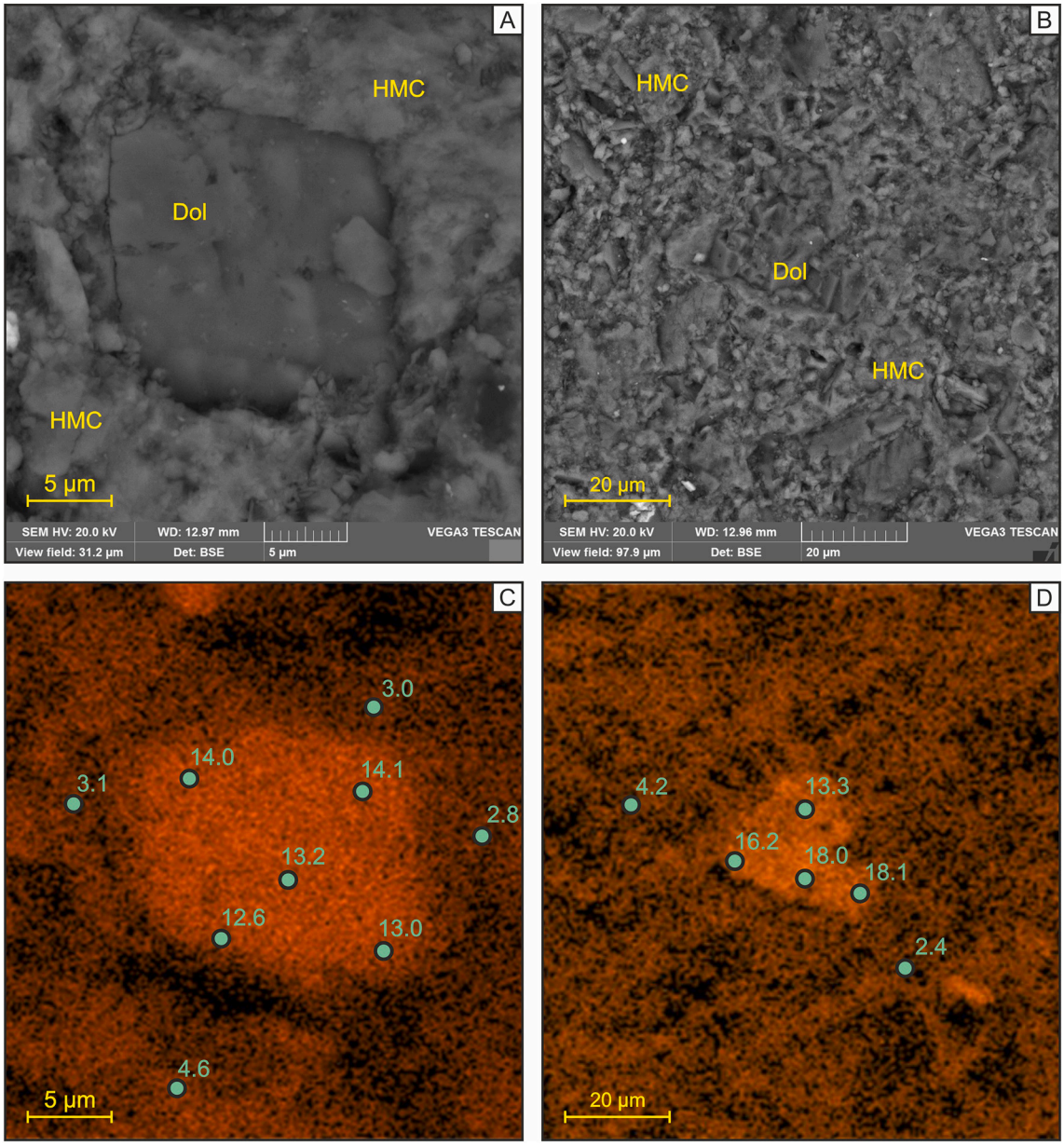

Fig. 5. (A and B) SEM-images of dolomite crystals incorporated in high magnesian calcite matrix: Dol – dolomite, HMC – high magnesian calcite. (C and D) Energy-dispersive X-ray spectroscopy maps of carbonate, revealing heterogeneous distribution of Mg. Green points show Mg content in %. (For interpretation of the references to colour in this figure legend, the reader is referred to the web version of this article.)

is often used to estimate the depth at which carbonate formation occurs (Himmler et al., 2015). The most common cold seeps carbonate minerals are high magnesium calcite (HMC), aragonite, and to lesser degree dolomite (Bayon et al., 2007; Crémière et al., 2012; Roberts et al., 2010). Aragonite formation occurs closer to the seafloor under high sulfate and oxygen and low sulfide concentrations, as sulfate concentration decreases in deeper sediments due to AOM (Aloisi et al., 2000; Bohrmann et al., 1998; Crémière et al., 2016). Conversely, HMC and dolomite preferably precipitate at depths several meters below the sediment-water interface (e.g., Tong et al., 2019). Furthermore, sulfate reduction in deeper sediments horizons promote the saturation of pore water with dissolved sulfide and intensify the HMC and dolomite mineralization due to the incorporation of Mg^{2+} ions into the calcite lattice (Zhang et al., 2012; Lu et al., 2018).

High magnesian calcite is the dominant carbonate mineral of studied carbonate samples collected from the Laptev Sea continental slope (Table 1). The carbonates were obtained using a grab sampler, which confirms their occurrence is shallowly below (<40 cm) the sediment-water interface. At high fluid flows SD-AOM often occurs in the upper horizon of sediments or even directly at the sediment-seawater interface and in this case, the pore waters are characterized by high concentrations of sulfate ions, which would cause aragonite precipitation (Luff et al., 2004; Teichert et al., 2005). However, the low bottom seawater temperature, combined with high flows of methane-content fluid, is a favorable factor for HMC formation (Burton and Walter, 1987). The association of pyrite and authigenic carbonate is related to the high activity of microbial sulfate reduction process during anaerobic oxidation of methane in a reducing environment during carbonate precipitation. Moreover, pyrite aggregates in the form of sunflowers and euhedral crystals indicate its formation in the deeper zones (Lin et al., 2016). In combination with the mineral composition and microcrystalline carbonate cement, this observation indicates that carbonate formation occurred in deeper sedimentary horizons. The seismic sections demonstrate clear forms in relief of seafloor, whose origin can associate

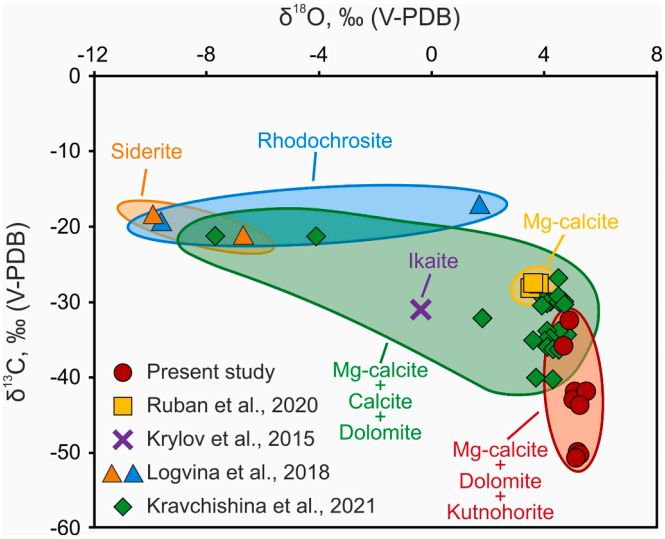

Fig. 6. Carbon and oxygen isotopic and mineral compositions of the studied carbonates from the Laptev Sea continental slope in comparison with authigenic carbonates from other areas of Laptev Sea: inner shelf (Krylov et al., 2015), outer shelf (Kravchishina et al., 2021; Ruban et al., 2020) and continental slope (Logvina et al., 2018).

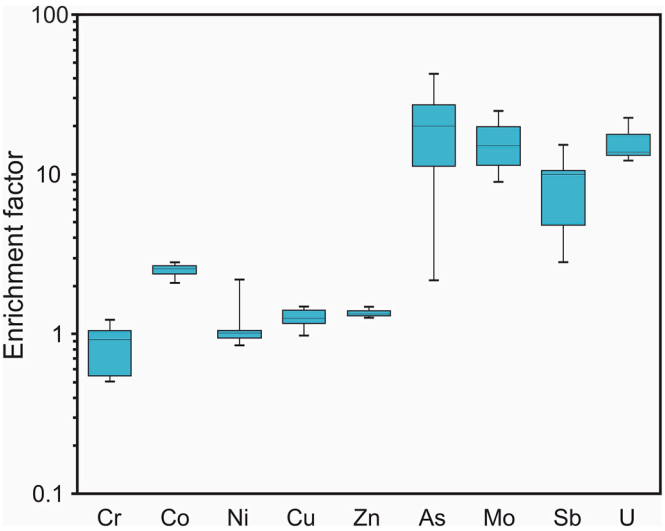

Fig. 7. Box and whiskers diagram demonstrating the enrichment factors of trace elements in the studied carbonates. Box boundaries mark 25th and 75th percentiles, horizontal lines within boxes show median, and whiskers indicate the minimums and maximums.

with mass-wasting (Bogoyavlensky et al., 2022). Mass-wasting processes could have contributed to the downslope movement of surficial sediments overlying carbonates. Thus, we suppose that the original zone of carbonate formation was deeper in the sediment column than the zone of their present-day occurrence (relative to the seafloor).

5.3. Trace elements

Besides stable isotope and mineralogical specifics, the elemental compositions of authigenic carbonates provide information about the environment of precipitation and trace fluid compositions (e.g., Feng et al., 2014; Hu et al., 2017; Liang et al., 2017). Some trace elements (e.g., Mo, U, As, Sb, Cr, V, Ni, Co, Zn, Pb) are redox-sensitive in marine sediments and they are enriched in anoxic conditions (Jacobs et al., 1985; Morford and Emerson, 1999; Sato et al., 2012; Tribovillard et al., 2006). Therefore, redox-sensitive elements are commonly used as reliable indicators to constrain variations in redox conditions during carbonate precipitation at cold seep sites (Deng et al., 2020; Feng and Chen, 2015; Ge et al., 2010; Peketi et al., 2012; Smrzka et al., 2019a; Smrzka et al., 2021). There are two hypotheses explaining the enrichment in trace elements: (1) iron and manganese oxyhydroxides in the water column scavenge trace elements from the seawater and deposit them to the surface sediments (shuttle effect; Tribovillard et al., 2013); (2) ascending seep fluid contribute to upward migration of trace elements due to pore water enrichment (Cangemi et al., 2010).

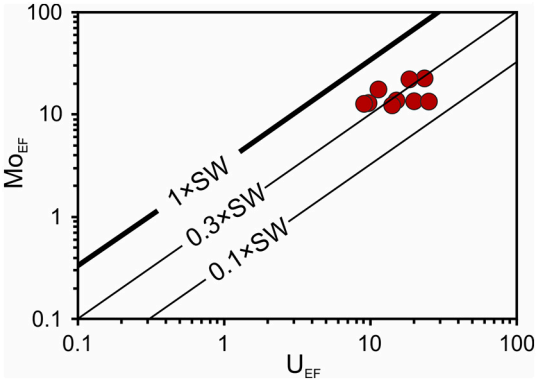

Fig. 8. Uranium and molybdenum covariation (Mo_{EF} versus U_{EF}) for the studied carbonates (modified from Algeo and Tribovillard (2009)). Samples are normalized using the Earth's upper crust compositions (McLennan, 2001). Lines show Mo/U ratios equal to the seawater value (1 × SW) and to fractions thereof (0.3 × SW, 0.1 × SW). $(Mo/U)_{SW} = 3.2$.

In this study, the values of Mo_{EF}, U_{EF}, As_{EF}, Co_{EF}, and Sb_{EF} show enrichment of carbonates in these elements (Table 3; Fig. 7). Trace elements form the order in terms of enrichment factor: As>Mo > U > Sb > Co. Interestingly, the arsenic enrichment exceeds the molybdenum enrichment, and the $(Mo/U)_{EF}$ ratio varies from 0.6 to 1.8, indicating similar enrichment in molybdenum and uranium. It is generally accepted that the accumulation of molybdenum in marine sediments occurs under anoxic (sulfide-rich) conditions. In contrast, the uranium accumulation occurs in suboxic conditions with low concentrations of oxygen and hydrogen sulfide (Algeo and Tribovillard, 2009). Cold-seep carbonates commonly form in an anoxic environment with high H_2S concentration, which is produced by the anaerobic oxidation of methane in the SMTZ. Anomalous high Mo concentrations (from 7.2 ppm to 21.7 ppm) and pyrite in carbonate cement (up to 2.5%; Table 1) can indicate that Fe sulfides are the main carriers of Mo. However, there is no correlation between the contents of pyrite and molybdenum in the studied carbonate samples (Fig. 9). At the same time, after removing an anomalous point on the cross-correlation plot of Mo and pyrite (sample 6939/6), the correlation coefficient (R^2) increases to 0.72. Probably, molybdenum is incorporated not only into iron sulfides but also into the clay-carbonate matrix, which is consistent with the results of the EDS analysis (Fig. 4). Since the mechanisms of molybdenum incorporation into carbonate minerals are still largely unknown and the sample for correlation analysis is small ($n = 9$), this observation should be treated with caution. As well as molybdenum, arsenic and antimony are incorporated into pyrite under sulfate-reducing environments (Morse and Luther, 1999). Therefore weak (for Sb) and strong (for As) correlations between pyrite and these trace elements contents support the role of iron sulfides in the accumulation of some redox-sensitive elements (Fig. 9). It should be noted that the results of scanning electron microscopy showed only authigenic phases of pyrite and the absence of detrital pyrite.

The enrichment of sediments and authigenic carbonates in molybdenum, arsenic, and antimony has already been noted for various marine settings and has been attributed to both shuttle transport (e.g., Hu

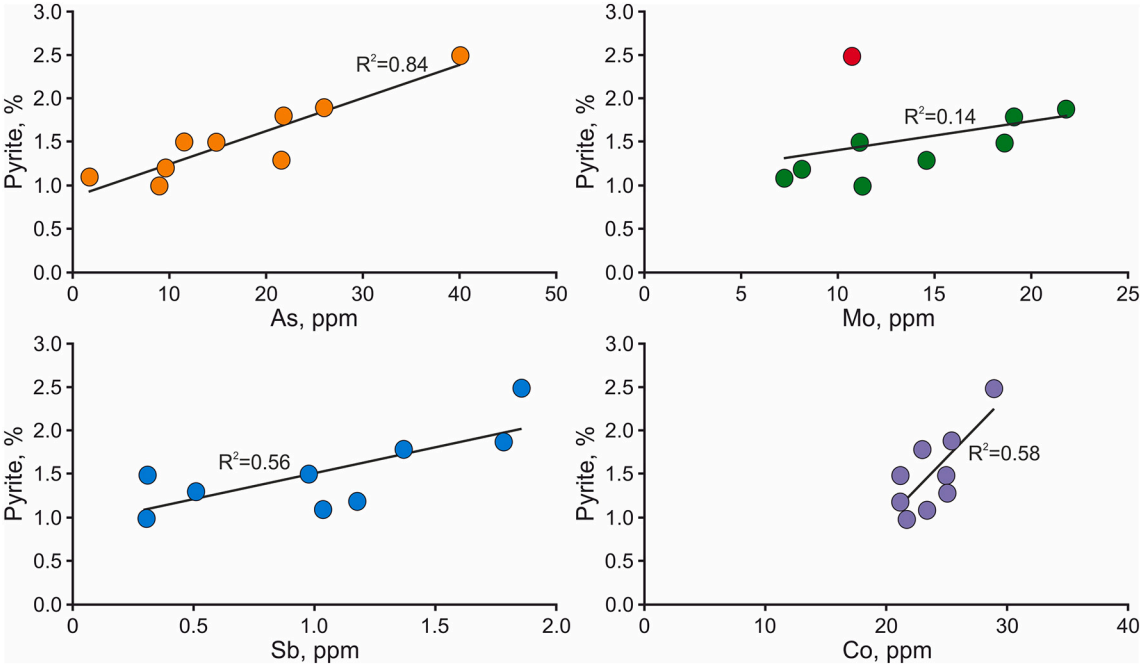

Fig. 9. Binary cross-correlation plots of trace elements and pyrite contents from the studied carbonates. Red circle shows an anomalous point on the cross-correlation plot of Mo and pyrite after removing which the correlation coefficient (R^2) increases to 0.72. (For interpretation of the references to colour in this figure legend, the reader is referred to the web version of this article.)

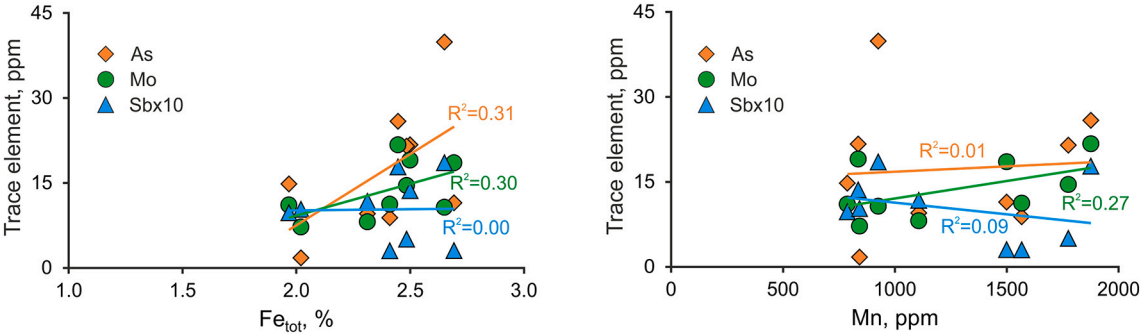

Fig. 10. Correlation between Fe_{tot}, Mn and As, Mo, and Sb contents of the studied authigenic carbonates from the continental slope of Laptev Sea. Sb concentrations have been multiplied by 10 for visual clarity.

Table 2
XRF major element contents (wt%) of the studied authigenic carbonates from the continental slope of Laptev Sea.

Sample	Na_2O	MgO	Al_2O_3	SiO_2	P_2O_5	K_2O	CaO	TiO_2	MnO	Fe_2O_{3tot}	LOI	Total	Detrital
6939/1	1.19	3.89	9.75	31.76	0.09	1.08	25.75	0.34	0.09	3.15	22.79	99.87	46.08
6939/2	1.19	3.55	8.81	31.49	0.05	1.07	22.04	0.34	0.09	3.02	28.11	99.76	44.73
6939/3	0.87	4.13	7.43	23.63	0.09	1.11	30.59	0.27	0.06	2.37	29.26	99.83	34.81
6939/4	0.87	3.82	8.09	25.43	0.09	0.81	28.98	0.32	0.13	3.22	28.04	99.81	37.87
6939/5	0.85	4.34	8.55	26.33	0.09	1.55	28.38	0.29	0.10	2.73	26.54	99.75	39.45
6939/6	1.25	3.82	9.56	34.96	0.09	1.42	22.76	0.38	0.09	3.77	21.53	99.64	50.09
6939/7	0.88	3.51	8.09	26.22	0.16	1.24	27.76	0.37	0.08	2.50	28.74	99.56	38.42
6939/8	0.98	3.75	7.93	24.41	0.09	0.97	28.54	0.31	0.17	2.97	29.51	99.64	36.59
6939/9	0.98	3.86	8.12	25.84	0.09	0.75	28.44	0.32	0.14	2.89	27.97	99.42	37.92

et al., 2014; Tribovillard et al., 2013) and ascending fluids (Cangemi et al., 2010; Nath et al., 2008). Iron and manganese oxyhydroxides, due to their sorption capacity, can act as carriers of Mo, As, and Sb transporting these elements from the seawater to the sediment by the shuttle effect (Scott and Lyons, 2012; Tribovillard et al., 2013; Tribovillard et al., 2006). However, this process only explains the enrichment in elements that can be sorbed by metal oxyhydroxides but it cannot explain the enrichment in uranium because it is poorly sorbed by Fe—Mn oxyhydroxides (Smrzka et al., 2020). Besides, the $(Mo/U)_{EF}$ ratio of carbonates, which formed lacking a contribution from deep ascending fluids, is much higher than that of seawater (Wang et al., 2019). Absence of correlations between Fe and Mn and Mo, As, and Sb contents in the studied carbonates (Fig. 10) indirectly eliminates the role of iron and manganese oxyhydroxide particulate shuttles for the

Table 3
Selected trace element contents (ppm) and enrichment factors of the studied authigenic carbonates from the continental slope of Laptev Sea.

	Cr	Co	Ni	Cu	Zn	As	Sb	Mo	Sr	Ba	Pb	Th	U
6939/1	52.2	22.9	26.6	21.2	59.1	21.7	1.36	19.0	721	290	10.1	5.91	24.6
6939/2	53.8	25.3	55.8	17.0	55.0	25.9	1.78	21.7	993	265	7.85	5.01	22.1
6939/3	22.3	21.1	22.1	15.4	44.4	14.8	0.97	11.1	961	232	7.42	5.53	19.0
6939/4	32.4	24.8	23.7	18.8	54.7	11.4	0.30	18.5	825	186	6.50	3.45	33.0
6939/5	23.6	21.1	21.0	13.7	56.1	9.52	1.17	8.13	884	238	8.25	5.41	20.8
6939/6	54.7	28.8	29.2	19.6	57.6	39.9	1.85	10.7	785	279	9.15	6.32	31.3
6939/7	22.4	23.3	21.7	14.9	49.5	1.73	1.03	7.20	834	223	7.94	5.68	19.2
6939/8	53.2	25.0	23.4	18.8	54.7	21.5	0.50	14.5	856	180	6.67	3.77	32.3
6939/9	41.0	21.6	30.1	19.8	51.6	8.83	0.30	11.2	852	191	6.56	3.99	18.4
	Cr_{EF}	Co_{EF}	Ni_{EF}	Cu_{EF}	Zn_{EF}	As_{EF}	Sb_{EF}	Mo_{EF}	Sr_{EF}	Ba_{EF}	Pb_{EF}	Th_{EF}	U_{EF}
6939/1	0.98	2.10	0.94	1.32	1.30	22.5	10.6	19.8	3.21	0.82	0.93	0.86	13.7
6939/2	1.12	2.57	2.19	1.17	1.34	29.7	15.3	25.0	4.89	0.83	0.80	0.81	13.6
6939/3	0.55	2.53	1.03	1.26	1.28	20.2	9.93	15.1	5.62	0.86	0.89	1.06	13.9
6939/4	0.73	2.74	1.01	1.41	1.45	14.3	2.84	23.2	4.43	0.64	0.72	0.61	22.7
6939/5	0.50	2.20	0.85	0.98	1.40	11.3	10.4	9.63	4.49	0.77	0.86	0.90	13.2
6939/6	1.05	2.69	1.06	1.25	1.29	42.3	14.7	11.3	3.57	0.81	0.86	0.94	17.8
6939/7	0.51	2.57	0.93	1.12	1.31	2.17	9.67	9.01	4.48	0.76	0.88	1.00	12.9
6939/8	1.23	2.82	1.02	1.44	1.48	27.4	4.82	18.6	4.69	0.63	0.75	0.67	22.1
6939/9	0.92	2.38	1.28	1.48	1.36	11.0	2.81	14.0	4.55	0.65	0.72	0.70	12.3

enrichments of Mo, As, and Sb. It is believed that ascending fluids not only deliver Mo, As, and Sb, but would also likely carry other elements (e.g., U, Cr, V, Ni, Co, Cu, Zn, Pb), resulting in carbonate enrichment in these elements (Tribovillard et al., 2013). Strong enrichment in U (U_{EF} from 12.3 to 22.7) and weak enrichment in cobalt (Co_{EF} from 2.1 to 2.8) are observed in studied carbonates (vanadium content was not measured). Thus, (i) U and Co enrichments, (ii) low values of $(Mo/U)_{EF}$ and (iii) the lack of correlations between iron, and manganese and Mo, As, and Sb contents indicate that ascending methane-bearing fluids played a crucial role in the enrichment of studied carbonates in As, Mo, Sb, U, Co at the Laptev Sea continental slope. However, additional input from the particulate shuttle process cannot be ruled out.

6. Conclusion

The authigenic carbonates collected from the Laptev Sea continental slope are mainly represented by high-magnesian calcite with $MgCO_3$ content from 9.1 mol% to 14.0 mol%. The negative carbon isotope composition of the samples suggests that carbonate formation was driven by the anaerobic oxidization of methane. The $\delta^{13}C$ values of carbonates (from −50.6 ‰ to −32.4 ‰ V-PDB) reveal a mixing of biogenic methane with carbon from other sources. High $\delta^{18}O$ values of the carbonates might be inherited from fluids enriched in ^{18}O due to dissociation gas hydrates, the presence of which in sedimentary cover has been recently predicted based on the seismic data analysis. The framboidal pyrite associated with the studied carbonate indicates the high activity of the microbial sulfate reduction during anaerobic oxidation of methane and the reducing environment of carbonate precipitation. The carbonates exhibit weak enrichment in cobalt, moderate and strong enrichments in arsenic, molybdenum, and antimony, and strong enrichments in uranium. As, Sb, and Co correlate with the content of authigenic pyrite, pointing at the role of iron sulfides in accumulating some redox-sensitive elements at cold seep sites. We propose that ascending methane-bearing fluids play an essential role in the enrichment of authigenic carbonates in As, Mo, Sb, and U at the Laptev Sea continental slope.

The study of authigenic carbonates from the continental slope of the Arctic Ocean provides ideal opportunities for the understanding periods and intensity of past methane release from underlying sources. Further studies should involve the use of radiogenic isotopes to assess carbonate mineral age and precipitation rates.

Declaration of Competing Interest

The authors declare that they have no known competing financial interests or personal relationships that could have appeared to influence the work reported in this paper.

Data availability

Data will be made available on request.

Acknowledgments

The research was supported by the Russian Science Foundation grants № 21-77-00033 (all laboratory investigations) and № 21-77-30001 (field hydroacoustic researches). Analytical studies were performed on the equipment acquired within the framework of the Tomsk Polytechnic University development program Priority 2030 (№ Priority2030-NIP/vneSP-021-1308-2022). We thank the Editor-in-Chief Oleg Pokrovsky and two anonymous reviewers for their constructive comments and suggestions, which greatly improved this paper.

References

Algeo, T.J., Tribovillard, N., 2009. Environmental analysis of paleoceanographic systems based on molybdenum-uranium covariation. Chem. Geol. 268, 211–225. https://doi.org/10.1016/j.chemgeo.2009.09.001.

Allouc, J., 1990. Quaternary crusts on slopes of the Mediterranean Sea: a tentative explanation for their genesis. Mar. Geol. 94, 205–238. https://doi.org/10.1016/0025-3227(90)90070-Z.

Aloisi, G., Pierre, C., Rouchy, J.M., Foucher, J.P., Woodside, J., 2000. Methane-related authigenic carbonates of Eastern Mediterranean Sea mud volcanoes and their possible relation to gas hydrate destabilisation. Earth Planet. Sci. Lett. 184, 321–338. https://doi.org/10.1016/S0012-821X(00)00322-8.

Baker, P.A., Burns, S.J., 1985. Occurrence and Formation of Dolomite in Organic-Rich Continental margin Sediments. Am. Assoc. Pet. Geol. Bull. 69, 1917–1930. https://doi.org/10.1306/94885570-1704-11D7-8645000102C1865D.

Baranov, B., Galkin, S., Vedenin, A., Dozorova, K., Gebruk, A., Flint, M., 2020. Methane seeps on the outer shelf of the Laptev Sea: characteristic features, structural control, and benthic fauna. Geo-Marine Lett. 1–17 https://doi.org/10.1007/s00367-020-00655-7.

Bates, N.R., Mathis, J.T., Cooper, L.W., 2009. Ocean acidification and biologically induced seasonality of carbonate mineral saturation states in the western Arctic Ocean. JGRC 114, C11007. https://doi.org/10.1029/2008JC004862.

Bauch, D., Cherniavskaia, E., Timokhov, L., 2016. Shelf basin exchange along the Siberian continental margin: Modification of Atlantic Water and lower Halocline Water. Deep Sea Res. Part I Oceanogr. Res. Pap. 115, 188–198. https://doi.org/10.1016/J.DSR.2016.06.008.

Bayon, G., Pierre, C., Etoubleau, J., Voisset, M., Cauquil, E., Marsset, T., Sultan, N., Le Drezen, E., Fouquet, Y., 2007. Sr/ca and Mg/ca ratios in Niger Delta sediments: Implications for authigenic carbonate genesis in cold seep environments. Mar. Geol. 241, 93–109. https://doi.org/10.1016/J.MARGEO.2007.03.007.

Bayon, G., Henderson, G.M., Bohn, M., 2009. U–Th stratigraphy of a cold seep carbonate crust. Chem. Geol. 260, 47–56. https://doi.org/10.1016/J.CHEMGEO.2008.11.020.

Berner, R.A., 1980. Early Diagenesis: A Theoretical Approach, p. 241.

Boetius, A., Ravenschlag, K., Schubert, C.J., Rickert, D., Widdel, F., Gleseke, A., Amann, R., Jørgensen, B.B., Witte, U., Pfannkuche, O., 2000. A marine microbial

consortium apparently mediating anaerobic oxidation methane. Nature 407, 623–626. https://doi.org/10.1038/35036572.
Bogoyavlensky, V., Kishankov, A., Yanchevskaya, A., Bogoyavlensky, I., 2018b. Forecast of gas hydrates distribution zones in the arctic ocean and adjacent offshore areas. Geosci. https://doi.org/10.3390/GEOSCIENCES8120453, 2018, Vol. 8, Page 453 8, 453.
Bogoyavlensky, V., Kishankov, A., Kazanin, A., Kazanin, G., 2022. Distribution of permafrost and gas hydrates in relation to intensive gas emission in the central part of the Laptev Sea (Russian Arctic). Mar. Pet. Geol. 138, 105527 https://doi.org/10.1016/j.marpetgeo.2022.105527.
Bogoyavlensky, V.I., Kazanin, G.S., Kishankov, A.V., 2018a. Bogoyavlensky: Dangerous gas-saturated objects in… - АкадеМия Google [WWW Document]. In: Drill. URL https://scholar.google.com/scholar_lookup?title=Dangerous+gas-saturated+objects+in+the+World+Ocean:+The+Laptev+Sea&author=Bogoyavlensky,+V.I.&author=Kazanin,+G.S.&author=Kishankov,+A.V.&publication_year=2018&journal=Drill.+Oil&volume=5&pages=20–29 (accessed 1.20.22).
Bohrmann, G., Greinert, J., Suess, E., Torres, M., 1998. Authigenic carbonates from the Cascadia subduction zone and their relation to gas hydrate stability. Geology 26, 647–650. https://doi.org/10.1130/0091-7613(1998)026<0647:ACFTCS>2.3.CO;2.
Botz, R., Wehner, H., Schmitt, M., Worthington, T.J., Schmidt, M., Stoffers, P., 2002. Thermogenic hydrocarbons from the offshore Calypso hydrothermal field, Bay of Plenty, New Zealand. Chem. Geol. 186, 235–248. https://doi.org/10.1016/S0009-2541(01)00418-1.
Burton, E.A., 1993. Controls on marine carbonate cement mineralogy: review and reassessment. Chem. Geol. 105, 163–179. https://doi.org/10.1016/0009-2541(93)90124-2.
Burton, E.A., Walter, L.M., 1987. Relative precipitation rates of aragonite and Mg calcite from seawater: temperature or carbonate ion control? Geology 15, 111–114. https://doi.org/10.1130/0091-7613(1987)15<111:RPROAA>2.0.CO;2.
Cangemi, M., Di Leonardo, R., Bellanca, A., Cundy, A., Neri, R., Angelone, M., 2010. Geochemistry and mineralogy of sediments and authigenic carbonates from the Malta Plateau, Strait of Sicily (Central Mediterranean): Relationships with mud/fluid release from a mud volcano system. Chem. Geol. 276, 294–308. https://doi.org/10.1016/j.chemgeo.2010.06.014.
Chuvilin, E., Bukhanov, B., Yurchenko, A., Davletshina, D., Shakhova, N., Spivak, E., Rusakov, V., Dudarev, O., Khaustova, N., Tikhonova, A., Gustafsson, O., Tesi, T., Martens, J., Jakobsson, M., Spasennykh, M., Semiletov, I., 2022. In-situ temperatures and thermal properties of the East Siberian Arctic shelf sediments: Key input for understanding the dynamics of subsea permafrost. Mar. Pet. Geol. 138, 105550 https://doi.org/10.1016/J.MARPETGEO.2022.105550.
Coplen, T.B., Kendall, C., Hopple, J., 1983. Comparison of stable isotope reference samples. Nature 302, 236–238.
Crémière, A., Pierre, C., Blanc-Valleron, M.M., Zitter, T., Çağatay, M.N., Henry, P., 2012. Methane-derived authigenic carbonates along the North Anatolian fault system in the Sea of Marmara (Turkey). Deep Sea Res. Part I Oceanogr. Res. Pap. 66, 114–130. https://doi.org/10.1016/J.DSR.2012.03.014.
Crémière, A., Lepland, A., Chand, S., Sahy, D., Kirsimäe, K., Bau, M., Whitehouse, M.J., Noble, S.R., Martma, T., Thorsnes, T., Brunstad, H., 2016. Fluid source and methane-related diagenetic processes recorded in cold seep carbonates from the Alvheim channel, Central North Sea. Chem. Geol. 432, 16–33. https://doi.org/10.1016/J.CHEMGEO.2016.03.019.
Daragan-Sushchova, L.A., Petrov, E.O., Petrov, O.V., Sobolev, N.N., 2021. Arctic Sedimentary Cover Structure and Eastern Arctic Structure Maps. In: Springer Geol, pp. 63–95. https://doi.org/10.1007/978-3-030-46862-0_3.
Davidson, D.W., Leaist, D.G., Hesse, R., 1983. Oxygen-18 enrichment in the water of a clathrate hydrate. Geochim. Cosmochim. Acta 47, 2293–2295. https://doi.org/10.1016/0016-7037(83)90053-4.
Deininger, M., Hansen, M., Fohlmeister, J., Schröder-Ritzrau, A., Burstyn, Y., Scholz, D., 2021. Are oxygen isotope fractionation factors between calcite and water derived from speleothems systematically biased due to prior calcite precipitation (PCP)? Geochim. Cosmochim. Acta 305, 212–227. https://doi.org/10.1016/J.GCA.2021.03.026.
Deng, Y., Chen, F., Hu, Y., Guo, Q., Cao, J., Chen, H., Zhou, J., Jiang, X., Zhu, J., 2020. Methane seepage patterns during the middle Pleistocene inferred from molybdenum enrichments of seep carbonates in the South China Sea. Ore Geol. Rev. 125, 103701 https://doi.org/10.1016/J.OREGEOREV.2020.103701.
Drachev, S.S., 2000. Laptev Sea rifted continental margin: Modern knowledge and unsolved questions. Polarforschung 68, 41–50.
Drachev, S.S., 2002. On the basement tectonics of the Laptev Sea shelf. Geotectonics 36, 483–497.
Dubinina, E.O., Miroshnikov, A.Y., Kossova, S.A., Shchuka, S.A., 2019. Modification of the Laptev Sea Freshened Shelf Waters based on Isotope and Salinity Relations. Geochem. Int. 57, 1–19. https://doi.org/10.1134/S001670291901004X.
Feng, D., Chen, D., 2015. Authigenic carbonates from an active cold seep of the northern South China Sea: New insights into fluid sources and past seepage activity. Deep. Res. Part II Top. Stud. Oceanogr. 122, 74–83. https://doi.org/10.1016/j.dsr2.2015.02.003.
Feng, D., Chen, D., Roberts, H.H., 2009. Petrographic and geochemical characterization of seep carbonate from Bush Hill (GC 185) gas vent and hydrate site of the Gulf of Mexico. Mar. Pet. Geol. 26, 1190–1198. https://doi.org/10.1016/j.marpetgeo.2008.07.001.
Feng, D., Roberts, H.H., Joye, S.B., Heydari, E., 2014. Formation of low-magnesium calcite at cold seeps in an aragonite sea. Terra Nova 26, 150–156. https://doi.org/10.1111/ter.12081.
Ge, L., Jiang, S.Y., Swennen, R., Yang, T., Yang, J.H., Wu, N.Y., Liu, J., Chen, D.H., 2010. Chemical environment of cold seep carbonate formation on the northern continental slope of South China Sea: evidence from trace and rare earth element geochemistry. Mar. Geol. 277, 21–30. https://doi.org/10.1016/j.margeo.2010.08.008.
Goldsmith, J., Graf, D., Heard, H., 1961. Lattice constants of the calcium magnesium carbonates. Am. Mineral. 46, 453–457.
Greinert, J., Bohrmann, G., Suess, E., 2001. Gas Hydrate-Associated Carbonates and Methane-Venting at Hydrate Ridge: Classification, distribution, and Origin of Authigenic Lithologies. In: Geophysical Monograph Series. Blackwell Publishing Ltd, pp. 99–113. https://doi.org/10.1029/GM124p0099.
Guan, H., Sun, Z., Mao, S., Xu, L., Cao, H., Geng, W., Xu, C., Zhang, X., Wu, N., 2019. Authigenic carbonate formation revealed by lipid biomarker inventory at hydrocarbon seeps: a case study from the Okinawa Trough. Mar. Pet. Geol. 101, 502–511. https://doi.org/10.1016/j.marpetgeo.2018.12.028.
Guinotte, J.M., Fabry, V.J., 2008. Ocean acidification and its potential effects on marine ecosystems. Ann. N. Y. Acad. Sci. 1134, 320–342. https://doi.org/10.1196/ANNALS.1439.013.
Haas, A., Peckmann, J., Elvert, M., Sahling, H., Bohrmann, G., 2010. Patterns of carbonate authigenesis at the Kouilou pockmarks on the Congo deep-sea fan. Mar. Geol. 268, 129–136. https://doi.org/10.1016/j.margeo.2009.10.027.
Hensen, C., Wallmann, K., Schmidt, M., Ranero, C.R., Suess, E., 2004. Fluid expulsion related to mud extrusion off Costa Rica - a window to the subducting slab. Geology 32, 201–204. https://doi.org/10.1130/G20119.1.
Hesse, R., 2003. Pore water anomalies of submarine gas-hydrate zones as tool to assess hydrate abundance and distribution in the subsurface: what have we learned in the past decade? Earth Sci. Rev. 61, 149–179. https://doi.org/10.1016/S0012-8252(02)00117-4.
Hesse, R., Harrison, W.E., 1981. Gas hydrates (clathrates) causing pore-water freshening and oxygen isotope fractionation in deep-water sedimentary sections of terrigenous continental margins. Earth Planet. Sci. Lett. 55, 453–462. https://doi.org/10.1016/0012-821X(81)90172-2.
Himmler, T., Birgel, D., Bayon, G., Pape, T., Ge, L., Bohrmann, G., Peckmann, J., 2015. Formation of seep carbonates along the Makran convergent margin, northern Arabian Sea and a molecular and isotopic approach to constrain the carbon isotopic composition of parent methane. Chem. Geol. 415, 102–117. https://doi.org/10.1016/j.chemgeo.2015.09.016.
Himmler, T., Sahy, D., Martma, T., Bohrmann, G., Plaza-Faverola, A., Bünz, S., Condon, D.J., Knies, J., Lepland, A., 2019. A 160,000-year-old history of tectonically controlled methane seepage in the Arctic. Sci. Adv. 5 https://doi.org/10.1126/SCIADV.AAW1450/SUPPL_FILE/AAW1450_SM.PDF.
Hood, A. Van S., Wallace, M.W., 2018. Neoproterozoic marine carbonates and their paleoceanographic significance. Glob. Planet. Chang. 160, 28–45. https://doi.org/10.1016/J.GLOPLACHA.2017.11.006.
Hu, Y., Feng, D., Peckmann, J., Roberts, H.H., Chen, D., 2014. New insights into cerium anomalies and mechanisms of trace metal enrichment in authigenic carbonate from hydrocarbon seeps. Chem. Geol. 381, 55–66. https://doi.org/10.1016/J.CHEMGEO.2014.05.014.
Hu, Y., Chen, L., Feng, D., Liang, Q., Xia, Z., Chen, D., 2017. Geochemical record of methane seepage in authigenic carbonates and surrounding host sediments: a case study from the South China Sea. J. Asian Earth Sci. 138, 51–61. https://doi.org/10.1016/j.jseaes.2017.02.004.
Jacobs, L., Emerson, S., Skei, J., 1985. Partitioning and transport of metals across the O2H2S interface in a permanently anoxic basin: Framvaren Fjord, Norway☆. Geochim. Cosmochim. Acta 49, 1433–1444. https://doi.org/10.1016/0016-7037(85)90293-5.
Kelts, K., McKenzie, J.A., 1982. Diagenetic dolomite formation in Quaternary anoxic diatomaceous muds of Deep Sea Drilling Project Leg 64, Gulf of California. In: Initial reports DSDP, Leg 64, Maz. to Long Beach, 1978-79. Part 2 553–569. https://doi.org/10.2973/DSDP.PROC.64.110.1982.
Kim, S.T., O'Neil, J.R., 1997. Equilibrium and nonequilibrium oxygen isotope effects in synthetic carbonates. Geochim. Cosmochim. Acta 61, 3461–3475. https://doi.org/10.1016/S0016-7037(97)00169-5.
Kravchishina, M.D., Lein, A.Y., Savvichev, A.S., Reykhard, L.E., Dara, O.M., Flint, M.V., 2017. Authigenic Mg-calcite at a cold methane seep site in the Laptev Sea. Oceanology 57, 174–191. https://doi.org/10.1134/S0001437017010064.
Kravchishina, M.D., Lein, A.Y., Flint, M.V., Baranov, B.V., Miroshnikov, A.Y., Dubinina, E.O., Dara, O.M., Boev, A.G., Savvichev, A.S., 2021. Methane-Derived Authigenic Carbonates on the Seafloor of the Laptev Sea Shelf, p. 8. https://doi.org/10.3389/fmars.2021.690304.
Krylov, A.A., Logvina, E.A., Matveeva, T.V., Prasolov, E.M., Sapega, V.F., Demidova, A. L., Radchenko, M.S., 2015. Ikaite (CaCO3 · 6H2O) in bottom sediments of the Laptev Sea and the role of anaerobic methane oxidation in this mineral- forming process. Russ. Soc. Lett. 4, 61–75. https://doi.org/10.7868/s002347611506020x.
Kulm, L.D., Suess, E., Moore, J.C., Carson, B., Lewis, B.T., Ritger, S.D., Kadko, D.C., Thornburg, T.M., Embley, R.W., Rugh, W.D., Massoth, G.J., Langseth, M.G., Cochrane, G.R., Scamman, R.L., 1986. Oregon subduction zone: Venting, Fauna, and carbonates. Science (80-.) 231, 561–566. https://doi.org/10.1126/SCIENCE.231.4738.561.
Lein, A.Y., 2004. Authigenic carbonate formation in the ocean. Lithol. Miner. Resour. 39, 1–30. https://doi.org/10.1023/B:LIMI.0000010767.52720.8F.
Li, J., Li, L., Bai, S., Ta, K., Xu, H., Chen, S., Pan, J., Li, M., Du, M., Peng, X., 2019. New insight into the biogeochemical cycling of methane, S and Fe above the Sulfate-methane transition Zone in methane hydrate-bearing sediments: a case study in the Dongsha area, South China Sea. Deep-Sea Res. I 145, 97–108.
Liang, Q., Hu, Y., Feng, D., Peckmann, J., Chen, L., Yang, S., Liang, J., Tao, J., Chen, D., 2017. Authigenic carbonates from newly discovered active cold seeps on the northwestern slope of the South China Sea: Constraints on fluid sources, formation

environments, and seepage dynamics. Deep. Res. Part I Oceanogr. Res. Pap 124, 31–41. https://doi.org/10.1016/j.dsr.2017.04.015.
Lin, Z., Sun, X., Peckmann, J., Lu, Y., Xu, L., Strauss, H., Zhou, H., Gong, J., Lu, H., Teichert, B.M., 2016. How sulfate-driven anaerobic oxidation of methane affects the sulfur isotopic composition of pyrite: a SIMS study from the South China Sea. Chem. Geol. 440, 26–41. https://doi.org/10.1016/j.chemgeo.2016.07.007.
Logvina, E., Krylov, A., Taldenkova, E., Blinova, V., Sapega, V., Novikhin, A., Kassens, H., Bauch, H.A., 2018. Mechanisms of late Pleistocene authigenic Fe–Mn-carbonate formation at the Laptev Sea continental slope (Siberian Arctic). Arktos 4, 1–13. https://doi.org/10.1007/s41063-018-0036-0.
Lu, Y., Sun, X., Xu, H., Konishi, H., Lin, Z., Xu, L., Chen, T., Hao, X., Lu, H., Peckmann, J., 2018. Formation of dolomite catalyzed by sulfate-driven anaerobic oxidation of methane: Mineralogical and geochemical evidence from the northern South China Sea. Am. Mineral. 103, 720–734.
Lu, Y., Yang, X., Lin, Z., Sun, X., Yang, Y., Peckmann, J., 2021. Reducing Microenvironments Promote Incorporation of Magnesium Ions into Authigenic Carbonate Forming at methane Seeps: Constraints for Dolomite Formation. Sedimentology 68, 2945–2964.Mansour, a.S., Sassen, R., 2011. Mineralogical and stable isotopic characterization of authigenic carbonate from a hydrocarbon seep site, Gulf of Mexico slope: possible relation to crude oil degradation. Mar. Geol. 281, 59–69. https://doi.org/10.1016/j.margeo.2011.02.004.
Luff, R., Wallmann, K., Aloisi, G., 2004. Numerical modeling of carbonate crust formation at cold vent sites: significance for fluid and methane budgets and chemosynthetic biological communities. Earth Planet. Sci. Lett. 221, 337–353. https://doi.org/10.1016/S0012-821X(04)00107-4.
Mansour, A.S., Sassen, R., 2011. Mineralogical and stable isotopic characterization of authigenic carbonate from a hydrocarbon seep site, Gulf of Mexico slope: possible relation to crude oil degradation. Marine Geol 281, 59–69.
Markgraf, S., Mineralogist, R.R.-A., 1985. undefined, 1985. In: High-Temperature Structure Refinements of Calcite and Magnesite. pubs.geoscienceworld.org, 70, 590400.
Martens, J., Wild, B., Muschitiello, F., O'Regan, M., Jakobsson, M., Semiletov, I., Dudarev, O.V., Gustafsson, Ö., 2020. Remobilization of dormant carbon from Siberian-Arctic permafrost during three past warming events. Sci. Adv. 6, 6546–6562. https://doi.org/10.1126/SCIADV.ABB6546/SUPPL_FILE/ABB6546_SM.PDF.
Matsumoto, R., 1990. Vuggy carbonate crust formed by hydrocarbon seepage on the continental shelf of Baffin Island, Northeast Canada. Geochem. J. 24, 143–158.
Mazzini, A., Svensen, H.H., Planke, S., Forsberg, C.F., Tjelta, T.I., 2016. Pockmarks and methanogenic carbonates above the giant Troll gas field in the Norwegian North Sea. Mar. Geol. 373, 26–38. https://doi.org/10.1016/j.margeo.2015.12.012.
McLennan, S.M., 2001. Relationships between the trace element composition of sedimentary rocks and upper continental crust. Geochem. Geophys. Geosyst. 2. https://doi.org/10.1029/2000GC000109.
Morford, J.L., Emerson, S., 1999. The geochemistry of redox sensitive trace metals in sediments. Geochim. Cosmochim. Acta 63, 1735–1750. https://doi.org/10.1016/S0016-7037(99)00126-X.
Morse, J.W., Luther, G.W., 1999. Chemical influences on trace metal-sulfide interactions in anoxic sediments. Geochim. Cosmochim. Acta 63, 3373–3378. https://doi.org/10.1016/S0016-7037(99)00258-6.
Naehr, T.H., Eichhubl, P., Orphan, V.J., Hovland, M., Paull, C.K., Ussler III, W., Lorenson, T.D., Greene, H.G., 2007. Authigenic carbonate formation at hydrocarbon seeps in continental margin sediments: A comparative study. Deep-sea Research Part II 54, 1268–1291.
Naehr, T.H., Rodriguez, N.M., Bohrmann, G., Paull, C.K., Botz, R., 2000. Methane-derived authigenic carbonates associated with gas hydrate decomposition and fluid venting above the Blake Ridge Diapir. In: Proceedings of the Ocean Drilling Program: Scientific Results. Texas A and M University, pp. 285–300. https://doi.org/10.2973/odp.proc.sr.164.228.2000.
Naehr, T.H., Birgel, D., Bohrmann, G., MacDonald, I.R., Kasten, S., 2009. Biogeochemical controls on authigenic carbonate formation at the Chapopote "asphalt volcano", Bay of Campeche. Chem. Geol. 266, 390–402. https://doi.org/10.1016/j.chemgeo.2009.07.002.
Nath, B., Jean, J.S., Lee, M.K., Yang, H.J., Liu, C.C., 2008. Geochemistry of high arsenic groundwater in Chia-Nan plain, Southwestern Taiwan: possible sources and reactive transport of arsenic. J. Contam. Hydrol. 99, 85–96. https://doi.org/10.1016/J.JCONHYD.2008.04.005.
Peckmann, J., Thiel, V., 2004. Carbon cycling at ancient methane-seeps. Chem. Geol. 205, 443–467. https://doi.org/10.1016/j.chemgeo.2003.12.025.
Peckmann, J., Reimer, A., Luth, U., Luth, C., Hansen, B.T., Heinicke, C., Hoefs, J., Reitner, J., 2001. Methane-derived carbonates and authigenic pyrite from the northwestern Black Sea. Mar. Geol. 177, 129–150. https://doi.org/10.1016/S0025-3227(01)00128-1.
Peketi, A., Mazumdar, A., Joshi, R.K., Patil, D.J., Srinivas, P.L., Dayal, A.M., 2012. Tracing the Paleo sulfate-methane transition zones and H2S seepage events in marine sediments: an application of C-S-Mo systematics. Geochem. Geophys. Geosyst. 13. https://doi.org/10.1029/2012GC004288.
Pierre, C., Blanc-Valleron, M.M., Demange, J., Boudouma, O., Foucher, J.P., Pape, T., Himmler, T., Fekete, N., Spiess, V., 2012. Authigenic carbonates from active methane seeps offshore Southwest Africa. Geo-Marine Lett. 32, 501–513. https://doi.org/10.1007/s00367-012-0295-x.
Polyakova, I.D., Borukaev, G.C., 2017. Structure and petroleum potential of the Laptev Sea region. Lithol. Miner. Resour. 52, 278–294. https://doi.org/10.1134/S0024490217040058.
Regnier, P., Dale, A.W., Arndt, S., LaRowe, D.E., Mogollón, J., Van Cappellen, P., 2011. Quantitative analysis of anaerobic oxidation of methane (AOM) in marine sediments: a modeling perspective. Earth Sci. Rev. 106, 105–130. https://doi.org/10.1016/J.EARSCIREV.2011.01.002.
Roberts, H.H., Feng, D., Joye, S.B., 2010. Cold-seep carbonates of the middle and lower continental slope, northern Gulf of Mexico. Deep. Res. Part II Top. Stud. Oceanogr. 57, 2040–2054. https://doi.org/10.1016/j.dsr2.2010.09.003.
Ruban, A., Rudmin, M., Dudarev, O., Mazurov, A., 2020. The formation of authigenic carbonates at a methane seep site in the northern part of the laptev sea. Minerals 10. https://doi.org/10.3390/min10110948.
Sackett, W.M., 1978. Carbon and hydrogen isotope effects during the thermocatalytic production of hydrocarbons in laboratory simulation experiments. Geochim. Cosmochim. Acta 42, 571–580. https://doi.org/10.1016/0016-7037(78)90002-9.
Sato, H., Hayashi, K.I., Ogawa, Y., Kawamura, K., 2012. Geochemistry of deep sea sediments at cold seep sites in the Nankai Trough: Insights into the effect of anaerobic oxidation of methane. Mar. Geol. 323–325, 47–55. https://doi.org/10.1016/j.margeo.2012.07.013.
Schier, K., Himmler, T., Lepland, A., Kraemer, D., Schönenberger, J., Bau, M., 2021. Insights into the REY inventory of seep carbonates from the Northern Norwegian margin using geochemical screening. Chem. Geol. 559, 119857 https://doi.org/10.1016/J.CHEMGEO.2020.119857.
Schubert, C.J., Nurnberg, D., Scheele, N., Pauer, F., Kriews, M., 1997. 13C isotope depletion in ikaite crystals: evidence for methane release from the Siberian shelves? Geo-Marine Lett. 17, 169–174. https://doi.org/10.1007/S003670050023.
Scott, C., Lyons, T.W., 2012. Contrasting molybdenum cycling and isotopic properties in euxinic versus non-euxinic sediments and sedimentary rocks: refining the paleoproxies. Chem. Geol. 324–325, 19–27. https://doi.org/10.1016/J.CHEMGEO.2012.05.012.
Sekretov, S.B., 2002. Structure and tectonic evolution of the Southern Eurasia Basin, Arctic Ocean. Tectonophysics 351, 193–243. https://doi.org/10.1016/S0040-1951(01)00278-5.
Sergienko, V.I., Lobkovskii, L.I., Semiletov, I.P., Dudarev, O.V., Dmitrievskii, N.N., Shakhova, N.E., Romanovskii, N.N., Kosmach, D.A., Nikol'Skii, D.N., Nikiforov, S.L., Salomatin, A.S., Anan'Ev, R.A., Roslyakov, A.G., Salyuk, A.N., Karnaukh, V.V., Chernykh, D.B., Tumskoi, V.E., Yusupov, V.I., Kurilenko, A.V., Chuvilin, E.M., Bukhanov, B.A., 2012. The degradation of submarine permafrost and the destruction of hydrates on the shelf of east arctic seas as a potential cause of the methane catastrophe: some results of integrated studies in 2011. Dokl. Earth Sci. 446, 1132–1137. https://doi.org/10.1134/S1028334X12080144.
Shakhova, N., Semiletov, I., Salyuk, A., Yusupov, V., Kosmach, D., Gustafsson, O., 2010. Extensive methane venting to the atmosphere from sediments of the East Siberian Arctic Shelf. Science 327, 1246–1250.
Shakhova, N., Semiletov, I., Sergienko, V., Lobkovsky, L., Yusupov, V., Salyuk, A., Salomatin, A., Chernykh, D., Kosmach, D., Panteleev, G., Nicolsky, D., Samarkin, V., Joye, S., Charkin, A., Dudarev, O., Meluzov, A., Gustafsson, O., 2015. The East Siberian Arctic Shelf: towards further assessment of permafrost-related methane fluxes and role of sea ice. Philos. Trans. R. Soc. A Math. Phys. Eng. Sci. 373, 20140451. https://doi.org/10.1098/rsta.2014.0451.
Shakhova, N., Semiletov, I., Chuvilin, E., 2019. Understanding the Permafrost–Hydrate system and associated methane releases in the east Siberian Arctic shelf. Geosciences 9, 251. https://doi.org/10.3390/geosciences9060251.
Shipilov, E.V., Lobkovsky, L.I., Shkarubo, S.I., 2019. Structure of the Khatanga–Lomonosov fracture zone according to seismic data. Dokl. Earth Sci. 487, 846–851. https://doi.org/10.1134/S1028334X19070286.
Smrzka, D., Zwicker, J., Bach, W., Feng, D., Himmler, T., Chen, D., Peckmann, J., 2019a. The behavior of trace elements in seawater, sedimentary pore water, and their incorporation into carbonate minerals: a review. Facies. https://doi.org/10.1007/S10347-019-0581-4, 2019 654 65, 1–47.
Smrzka, D., Zwicker, J., Misch, D., Walkner, C., Gier, S., Monien, P., Bohrmann, G., Peckmann, J., 2019b. Oil seepage and carbonate formation: a case study from the southern Gulf of Mexico. Sedimentology 66, 2318–2353. https://doi.org/10.1111/sed.12593.
Smrzka, D., Feng, D., Himmler, T., Zwicker, J., Hu, Y., Monien, P., Tribovillard, N., Chen, D., Peckmann, J., 2020. Trace elements in methane-seep carbonates: potentials, limitations, and perspectives. Earth Sci. Rev. 208, 103263.
Smrzka, D., Zwicker, J., Lu, Y., Sun, Y., Feng, D., Monien, P., Bohrmann, G., Peckmann, J., 2021. Trace element distribution in methane-seep carbonates: the role of mineralogy and dissolved sulfide. Chem. Geol. 580, 120357 https://doi.org/10.1016/J.CHEMGEO.2021.120357.
Sofer, Z., Gat, J.R., 1975. The isotope composition of evaporating brines: effect of the isotopic activity ratio in saline solutions. Earth Planet. Sci. Lett. 26, 179–186. https://doi.org/10.1016/0012-821X(75)90085-0.
Sun, Y., Gong, S., Li, N., Peckmann, J., Jin, M., Roberts, H.H., Chen, D., Feng, D., 2020. A new approach to discern the hydrocarbon sources (oil vs. methane) of authigenic carbonates forming at marine seeps. Mar. Pet. Geol. 114, 104230 https://doi.org/10.1016/j.marpetgeo.2020.104230.
Tarutani, T., Clayton, R.N., Mayeda, T.K., 1969. The effect of polymorphism and magnesium substitution on oxygen isotope fractionation between calcium carbonate and water. Geochim. Cosmochim. Acta 33, 987–996. https://doi.org/10.1016/0016-7037(69)90108-2.
Teichert, B.M.A., Bohrmann, G., Suess, E., 2005. Chemoherms on Hydrate Ridge - Unique microbially-mediated carbonate build-ups growing into the water column. Palaeogeogr. Palaeoclimatol. Palaeoecol. 227, 67–85. https://doi.org/10.1016/j.palaeo.2005.04.029.
Thiagarajan, N., Crémière, A., Blättler, C., Lepland, A., Kirsimäe, K., Higgins, J., Brunstad, H., Eiler, J., 2020. Stable and clumped isotope characterization of authigenic carbonates in methane cold seep environments. Geochim. Cosmochim. Acta 279, 204–219. https://doi.org/10.1016/j.gca.2020.03.015.

Tong, H., Feng, D., Cheng, H., Yang, S., Wang, H., Min, A.G., Edwards, R.L., Chen, Z., Chen, D., 2013. Authigenic carbonates from seeps on the northern continental slope of the South China Sea: New insights into fluid sources and geochronology. Mar. Pet. Geol. 43, 260–271. https://doi.org/10.1016/j.marpetgeo.2013.01.011.

Tong, H., Feng, D., Peckmann, J., Roberts, H.H., Chen, L., Bian, Y., Chen, D., 2019. Environments favoring dolomite formation at cold seeps: a case study from the Gulf of Mexico. Chem. Geol. 518, 9–18.

Tribovillard, N., Algeo, T.J., Lyons, T., Riboulleau, A., 2006. Trace metals as paleoredox and paleoproductivity proxies: an update. Chem. Geol. 232, 12–32. https://doi.org/10.1016/j.chemgeo.2006.02.012.

Tribovillard, N., du Châtelet, E.A., Gay, A., Barbecot, F., Sansjofre, P., Potdevin, J.L., 2013. Geochemistry of cold seepage-impacted sediments: Per-ascensum or per-descensum trace metal enrichment? Chem. Geol. 340, 1–12. https://doi.org/10.1016/j.chemgeo.2012.12.012.

Ussler, W., Paull, C.K., 1995. Effects of ion exclusion and isotopic fractionation on pore water geochemistry during gas hydrate formation and decomposition. Geo-Mar. Lett. https://doi.org/10.1007/BF01204496, 1995 151 15, 37–44.

Veizer, J., 1983. Chemical diagenesis of carbonates: theory and application of trace element technique. In: Stable Isotope in Sedimentary Geology, 10. SEPM Short Course, pp. 3–100.

Wang, Q., Chen, D., Peckmann, J., 2019. Iron shuttle controls on molybdenum, arsenic, and antimony enrichment in Pliocene methane-seep carbonates from the southern Western Foothills, Southwestern Taiwan. Mar. Pet. Geol. 100, 263–269. https://doi.org/10.1016/j.marpetgeo.2018.11.011.

Whiticar, M.J., Faber, E., Schoell, M., 1986. Biogenic methane formation in marine and freshwater environments: CO2 reduction vs. acetate fermentation-Isotope evidence. Geochim. Cosmochim. Acta 50, 693–709. https://doi.org/10.1016/0016-7037(86)90346-7.

Wilkin, R.T., Barnes, H.L., 1996. Pyrite formation by reactions of ion monosulfides with dissolved inorganic and organic sulfur species. Geochim. Cosmochim. Ac. 60, 4167–4179.

Yao, H., Panieri, G., Lehmann, M.F., Himmler, T., Niemann, H., 2021. Biomarker and isotopic composition of seep carbonates record environmental conditions in two Arctic methane Seeps. Front. Earth Sci. 8 https://doi.org/10.3389/FEART.2020.570742/FULL.

Zhang, F., Xu, H., Konishi, H., Roden, E.E., 2010. A relationship between d104 value and composition in the calcite-disordered dolomite solid-solution series. Am. Mineral. 95, 1650–1656. https://doi.org/10.2138/am.2010.3414.

Zhang, F., Xu, H., Konishi, H., Kemp, J.M., Roden, E.E., Shen, Z., 2012. Dissolved sulfide-catalyzed precipitation of disordered dolomite: Implications for the formation mechanism of sedimentary dolomite. Geochim. Cosmochim. Acta 97, 148–165. https://doi.org/10.1016/J.GCA.2012.09.008.

Zhou, C., Guan, C., Cui, H., Ouyang, Q., Wang, W., 2016. Methane-derived authigenic carbonate from the lower Doushantuo Formation of South China: Implications for seawater sulfate concentration and global carbon cycle in the early Ediacaran Ocean. Palaeogeogr. Palaeoclimatol. Palaeoecol. 461, 145–155. https://doi.org/10.1016/j.palaeo.2016.08.017.